MOLECULAR IMAGING AND BIOLOGY

Mol Imaging Biol (2019) 21:491–499
DOI: 10.1007/s11307-018-1242-7

Published Online: 30 August 2018

RESEARCH ARTICLE

Apoptotic PET Imaging of Rat Pulmonary Fibrosis with Small-Molecule Radiotracer

Ying Xiong, Dahong Nie, Shaoyu Liu, Hui Ma, Shu Su, Aixia Sun, Jing Zhao, Zhanwen Zhang, Xianhong Xiang, Ganghua Tang

Department of Medical Imaging and Guangdong Engineering Research Center for Translational Application of Medical Radiopharmaceuticals, The First Affiliated Hospital, Sun Yat-sen University, 58 Zhongshan Road II, Guangzhou, 510080, China

Abstract

Purpose: The purpose of this study was to assess the potential utility of small-molecule apoptotic radiotracer, 2-(5-[^{18}F]fluoropentyl)-2-methyl malonic acid ([^{18}F]ML-10), for positron emission tomography (PET)/computed tomography (CT) monitoring the progression of pulmonary fibrosis in a rat model.

Procedures: Male Sprague-Dawley rats were used to establish a rat model of pulmonary fibrosis by means of bleomycin (BLM) administration; control rats received saline ($n = 12$ per group). PET/CT with [^{18}F]ML-10 and 2-deoxy-2-[^{18}F]fluoro-D-glucose ([^{18}F]FDG) was performed in two groups at different stages of pulmonary fibrosis. The fibrotic response and the cell apoptosis were assessed with histologic examination. Differences in the apoptosis rate, fibrotic activity, and the lung uptake of [^{18}F]ML-10 and [^{18}F]FDG between two groups were determined with Student *t* test.

Results: Compared with control group, BLM group showed a higher lung uptake of [^{18}F]ML-10 at all imaging time points (all $P < 0.001$). During the fibrotic phase of this disease model (days 21 and 28), the lung uptake of [^{18}F]ML-10 was higher than that of [^{18}F]FDG in the BLM group (all $P < 0.001$). Moreover, accumulation of [^{18}F]ML-10 in the lung tissues increased in proportion to the apoptosis rate ($R^2 = 0.9863$, $P < 0.0001$) and fibrotic activity ($R^2 = 0.9631$, $P < 0.0001$) of rat pulmonary fibrosis. Conversely, no correlation between [^{18}F]FDG uptake and fibrotic activity was found.

Conclusions: [^{18}F]ML-10 PET/CT enabled monitoring the progression of rat pulmonary fibrosis, whereas [^{18}F]FDG PET/CT could not. Implications for noninvasive diagnosis of pulmonary fibrosis, assessment of fibrotic activity, and evaluation of antifibrotic therapy are expected.

Key words: Pulmonary fibrosis, Bleomycin, PET/CT, [^{18}F]ML-10, [^{18}F]FDG

Introduction

Idiopathic pulmonary fibrosis (IPF) is a progressive and lethal disease characterized by diffuse interstitial fibrosis with excessive deposition of collagens and extracellular matrix proteins eventually resulting in destruction of the lung architecture and severe insufficient pulmonary functions [1–3]. For IPF patients, the prognosis is poor with a median survival of 2 to 5 years [4]. The pathogenesis of IPF is unknown [1]. Although inflammation is present in IPF lungs, it does not seem to play an important role in the pathogenesis of this disease given that anti-inflammatory therapies have been shown to be ineffective [5, 6].

The early diagnosis and accurate staging of pulmonary fibrosis are vital for measuring disease activity, improving

Ying Xiong and Dahong Nie contributed equally to this work.

Correspondence to: Xianhong Xiang; *e-mail:* xxianhong@mail.sysu.edu.cn, Ganghua Tang; *e-mail:* tangghua@mail.sysu.edu.cn

patient care, and evaluating the effect of antifibrotic therapy. High-resolution computed tomography (HRCT) and lung biopsy are the current reference standard in the diagnosis of pulmonary fibrosis. However, lung biopsy is invasive and HRCT indicates abnormal pulmonary density but cannot assess disease activity [2]. Compared with HRCT, positron emission tomography (PET)/computed tomography (CT) could provide both anatomical and functional imaging information of diseases [7]. Recent studies evaluated the clinical value of PET/CT in the diagnosis of pulmonary fibrosis in IPF patients and animal models, mostly with 2-deoxy-2-[^{18}F]fluoro-D-glucose ([^{18}F]FDG). Although high uptake of [^{18}F]FDG was observed in IPF lungs, it seemed to be more associated with inflammatory changes as a peak of [^{18}F]FDG uptake was observed at the early inflammatory phase of pulmonary fibrosis and it decreased during the later fibrotic phase [6, 8–19].

Apoptosis is a cell death process whose dysfunction plays an important role in the etiology of numerous diseases [20]. Recent studies demonstrated that apoptotic type II pneumocyte death was observed in IPF lungs and apoptosis of type II pneumocytes could be an important factor in the pathogenesis of this disease [21, 22]. Aposense family was a set of novel small-molecule probes and it accumulated selectively in the apoptotic cells. 2-(5-[^{18}F]Fluoropentyl)-2-methyl malonic acid ([^{18}F]ML-10) was a member of Aposense family and was able to selectively target apoptotic cells [23]. Therefore, we hypothesized that apoptotic PET imaging with [^{18}F]ML-10 could be used for noninvasive detection of pulmonary fibrosis and assessment of disease activity in a rat model. Bleomycin (BLM) induction is the most commonly used method to generate pulmonary fibrosis in animal models. Recent studies showed that obvious pulmonary fibrosis was observed at day 14 after a single intratracheal injection of BLM [6, 24].

In this study, the aim was to assess the potential utility of small-molecule apoptotic radiotracer, [^{18}F]ML-10, for PET/CT monitoring the progression of pulmonary fibrosis in a rat model.

Materials and Methods

Rat Model of Lung Fibrosis

All animal experiments were performed on rats anesthetized with 2 % pentobarbital sodium (0.225 ml/kg) according to a protocol approved by the animal ethical and welfare committee. Six-week-old male Sprague-Dawley rats were used in these experiments. They were housed under specific pathogen-free conditions with free access to food and water.

We established a rat model of pulmonary fibrosis by a single intratracheal instillation of BLM as previously described [25]. In the BLM group, rats were instilled with 5 mg/kg BLM (Bleomycin Hydrochloride for Injection, Nippon Kayaku) diluted in sterile saline solution. Rats in the control group were treated with saline. At days 7, 14, 21, and 28 after instillation, three rats from each group were used for PET/CT with [^{18}F]ML-10 and [^{18}F]FDG, respectively. After PET/CT scans, rats were sacrificed by exsanguination under deep anesthesia to harvest the lung samples for further investigations.

Small-Animal PET/CT Imaging

[^{18}F]ML-10 PET/CT Imaging

To study the correlation between cell apoptosis and the progression of pulmonary fibrosis, [^{18}F]ML-10 PET/CT imaging was performed at 7, 14, 21, and 28 days after administration of BLM or saline ($n = 6$ per time point, three rats in the BLM group and three in the control group). [^{18}F]ML-10 was synthesized in the radiochemical purity of over 95 % and the specific activity of about 65.8 GBq/μmol, at our PET-CT center according to the method 1 reported by Liu et al. [26]. Rats were injected intravenously with [^{18}F]ML-10 solution (37 MBq/kg). PET/CT imaging was performed at 60 min after injection.

For a comparative study, [^{18}F]FDG PET/CT was also performed at 7, 14, 21, and 28 days after instillation ($n = 6$ per time point, three rats in the BLM group and three in the control group). Rats were fasted for over 4 h before injection of [^{18}F]FDG. The rats received an intravenous injection of [^{18}F]FDG solution (37 MBq/kg) 60 min before imaging.

Anesthetized rats were positioned in an Inveon small-animal PET/CT scanner (Siemens, Knoxville, TN), and the lungs centered in the field of view. Imaging acquisition started with a low-dose CT scan, which was used for attenuation correction and localization of the lesion site. Then, a 10-min PET scan followed immediately. After the reconstruction of PET/CT images with two-dimensional ordered-subsets expectation maximum (OSEM), the regions of interest (ROIs) were drawn over the lesion site of lung on each PET/CT image by using Inveon Research Workplace 4.1 software. Mean radioactivity within each region of interest was measured to quantify the uptake of [^{18}F]ML-10 or [^{18}F]FDG expressed as standardized uptake value (SUV).

Quantitative Analysis of Pulmonary Fibrosis

The Ashcroft score of lung fibrosis was used to estimate the severity of pulmonary fibrosis [27]. At days 7, 14, 21, and 28, three rats from each group were sacrificed to harvest the lung samples. Lung samples were fixed with 4 % paraformaldehyde, embedded in paraffin, and 4-μm sections were prepared for Masson trichrome staining. At day 21, the grade of lung fibrosis was scored for each lung by calculating the mean of the fibrotic changes on six different fields (magnification × 40) according to the method described by Ashcroft et al. [27].

Lung collagen content was assessed by measuring hydroxyproline (HYP), a major component of collagen [6, 24, 28]. At days 7, 14, 21, and 28, HYP was quantified by using an HYP assay kit (Sigma-Aldrich, USA) according to the manufacturer's instructions ($n = 6$ per time point, three rats in the BLM group and three in the control group). Data were expressed as micrograms of HYP per milligram wet lung tissue (μg/mg).

Apoptosis Detection

Immunofluorescence staining was performed to determine the presence of apoptotic cells in lung sections. Apoptosis was examined by the terminal deoxynucleotidyl transferase-mediated dUTP nick-end labeling (TUNEL) assay using the *in situ* cell death detection kit (Roche, Germany). At day 21, lung sample slices (4 μm thick) obtained from BLM-treated rats and control rats were stained with TUNEL and 4′,6-diamidino-2-phenylindole (DAPI) probe (three rats per group).

Apoptosis rate was quantitative assessed by flow cytometry (FCM) to further explore the correlation between apoptosis and pulmonary fibrosis. At days 7, 14, 21, and 28, lung samples ($n = 6$ per time point, three rats in the BLM group and three in the control group) were collected. Briefly, the lungs were rinsed with phosphate-buffered saline (PBS), minced with micro scissors, and enzymatically digested and filtered through 200-mesh nylon net. After centrifugation, lung cellular samples were collected and apoptosis rates of cells were measured using a FITC Annexin V apoptosis detection kit (BD, USA) *via* a flow cytometry (guava easyCyte, EMD Millipore Corporation). All data were processed with guavaSoft.

Statistical Analysis

Statistical analysis of single comparison between the two groups was determined using two-tailed Student *t* test by Prism software (V6.0; GraphPad, La Jolla) and SPSS software (V20.0; SPSS Inc., IBM). For all tests, quantitative data were expressed as means ± standard deviations and a *P* value of less than 0.05 was considered indicative of a statistically significant difference.

Results

Significant Lung Fibrosis with Corresponding Apoptosis in BLM-Treated Rats

A significant increase of fibrosis was observed around days 21–28 after administration of BLM, including aberrant proliferation of fibroblasts, thickening of alveolar septa, and destruction of alveolar structure (Fig. 1a). Lung HYP content was measured from the control and BLM groups to assess the dynamic changes of collagen content. After administration of BLM, lung HYP content represented a dramatically and consistently increasing trend compared with control rats from day 7 to day 28 (all $P < 0.05$) (Fig. 1b). Compared with the control group, the BLM group showed a higher degree of pulmonary fibrosis at day 21 (0.50 ± 0.17 *vs.* 6.17 ± 0.76, respectively; $P < 0.001$) (Fig. 1c).

At day 21, an increased number of apoptotic cells were observed in the lung tissues of BLM-treated rats, as compared with control rats (Fig. 2). At different time points, the apoptosis rate of lung tissues obtained from the two groups was determined by flow cytometry. The results showed that the rate of apoptotic cells in BLM-treated rats was significantly higher than that in control rats (all $P < 0.001$) and apoptosis rate of the rat pulmonary fibrosis models from BLM-treated rats was found to occur in a positive time-dependent manner (Fig. 3).

[^{18}F]ML-10 PET/CT Imaging

In order to investigate whether PET/CT imaging of [^{18}F]ML-10 could be applied to monitor the severity of pulmonary fibrosis, the uptake of [^{18}F]ML-10 in lung tissues was analyzed for comparisons between the two groups at different time points. At day 28, CT images showed areas of consolidation in lung tissues after BLM administration and [^{18}F]ML-10 uptake was marked noticed in consolidation areas of the lungs, which were characterized by the reticulation and honeycombing (Fig. 4a). The uptake of [^{18}F]ML-10 in lung tissues was monitored at different stages of this disease in both the BLM and control groups (Fig. 4b). Compared with control rats, BLM-treated rats showed a higher [^{18}F]ML-10 uptake starting at day 7 after instillation (SUV, 0.18 ± 0.02 *vs.* 0.42 ± 0.04, respectively; $P < 0.001$). At day 14, the difference of [^{18}F]ML-10 uptake between the BLM and control groups became more significant (SUV, 0.65 ± 0.03 *vs.* 0.22 ± 0.03, respectively; $P < 0.001$). The higher [^{18}F]ML-10 uptake in the BLM group was still present in the later fibrotic phase of this disease and represented a consistently increasing trend compared with the control group from day 21 (SUV, 0.94 ± 0.06 *vs.* 0.19 ± 0.01, respectively; $P < 0.001$) to day 28 (SUV, 1.25 ± 0.05 *vs.* 0.20 ± 0.01, respectively; $P < 0.001$).

[^{18}F]FDG PET/CT Imaging

We assessed the relationship between glucose metabolism and the severity of fibrosis in the lung tissues with [^{18}F]FDG PET/CT imaging. [^{18}F]FDG was found to be distributed in lesion areas of the lungs in BLM-treated rats, compared with control rats (Fig. 5a). We continuously monitored the uptake of [^{18}F]FDG in the lung tissues from day 7 to day 28 in both the BLM and control groups (Fig. 5b). Starting at day 7 after instillation, a significantly higher [^{18}F]FDG uptake of lung tissue

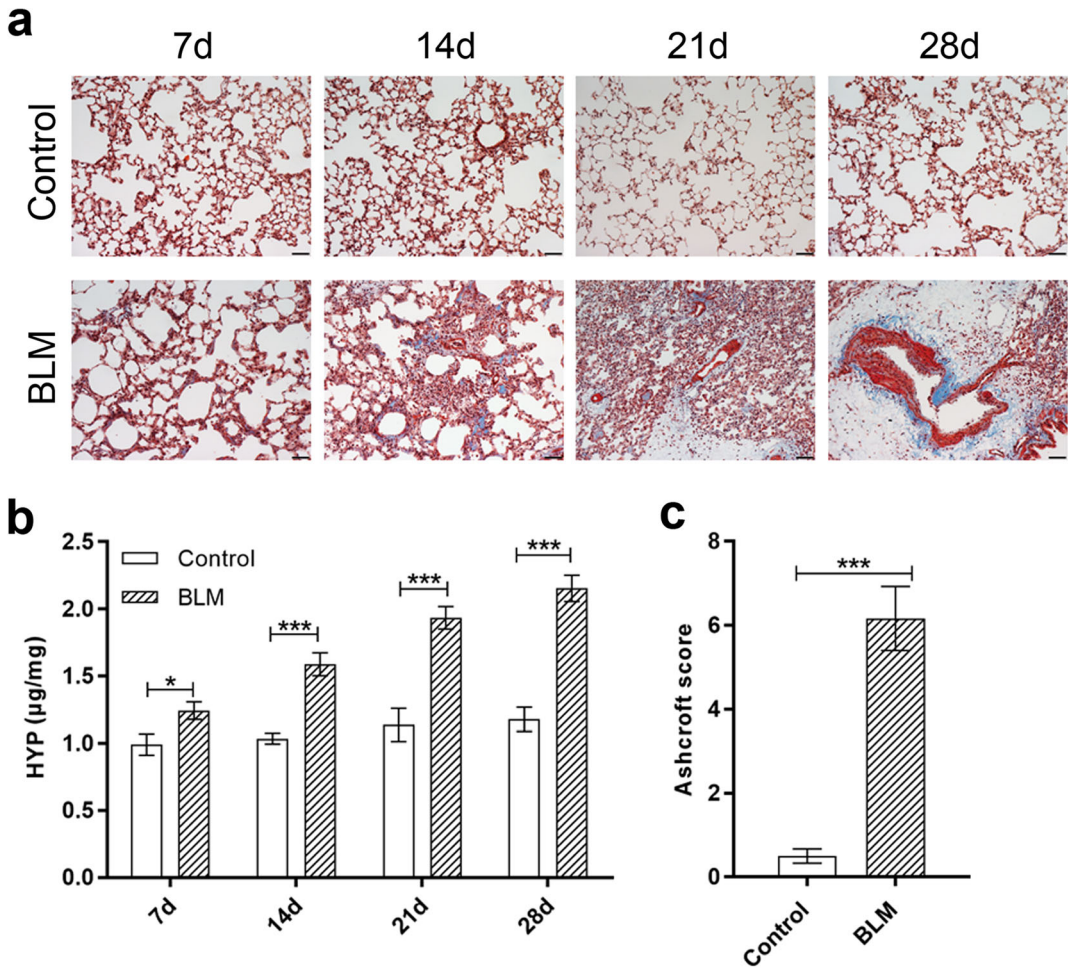

Fig. 1. Histologic changes and collagen deposition in the control and BLM groups. **a** Representative sections of lungs stained with Masson trichrome (magnification, × 200) obtained 7, 14, 21, and 28 days after administration of saline or BLM. **b** Lung HYP content at 7, 14, 21, and 28 days after instillation ($n = 3$ per group for days 7, 14, 21, and 28, respectively). **c** The grade of lung fibrosis was scored according to the method described by Ashcroft. Ashcroft score of fibrosis was measured at 21 days after instillation of saline or BLM ($n = 3$ per group). All data are given as means ± standard deviations. $^{*}P < 0.05$, $^{**}P < 0.01$, $^{***}P < 0.001$. Scale bars = 50 μm. *BLM* bleomycin.

was observed in BLM-treated rats, as compared with control rats (SUV, 0.60 ± 0.04 *vs* 0.20 ± 0.02, respectively; $P < 0.001$). The higher [^{18}F]FDG uptake in the BLM group reaching a peak value at day 14 (SUV, 0.81 ± 0.06 *vs.* 0.19 ± 0.04, respectively; $P < 0.001$). However, the [^{18}F]FDG uptake in BLM-treated rats was decreased from day 21 to day 28 after instillation, but was higher than in control rats at day 21 (SUV, $0.6\ 5 \pm 0.04$ *vs.* 0.22 ± 0.03, respectively; $P < 0.001$) and day 28 (SUV, 0.50 ± 0.04 *vs.* 0.23 ± 0.01, respectively; $P < 0.001$). Furthermore, the lung uptake was also analyzed for comparisons between [^{18}F]ML-10 PET and [^{18}F]FDG PET at days 21 and 28 after BLM instillation. During the fibrotic phase of this disease model, the lung uptake of [^{18}F]ML-10 was higher than that of [^{18}F]FDG in the BLM group from day 21 (SUV, 0.94 ± 0.06 *vs.* 0.65 ± 0.04, respectively; $P < 0.001$) to day 28 (SUV, 1.25 ± 0.05 *vs.* 0.50 ± 0.04, respectively; $P < 0.001$) (Fig. 5c).

Correlations

We analyzed the relationship between the uptake of [^{18}F]ML-10, [^{18}F]FDG and the severity of lung fibrosis in BLM-treated rats. At days 7, 14, 21, and 28, longitudinal PET imaging with [^{18}F]ML-10 and [^{18}F]FDG was performed along the progression of the rat pulmonary fibrosis model. After PET/CT with both radiotracers, lung collagen content and apoptosis rate were assessed with histologic examination of lung sections in BLM-treated rats at days 7, 14, 21, and 28 after instillation. A strong correlation was found between apoptosis rate and lung HYP content ($R^2 = 0.9353$, $P < 0.0001$) (Fig. 6a), a specific component of tissue collagen and fibrosis marker [6, 24, 28]. As a typical PET radiotracer for apoptosis imaging, the [^{18}F]ML-10 uptake in BLM-treated rats showed a strong positive correlation with apoptosis rate ($R^2 = 0.9863$, $P < 0.0001$) (Fig. 6b) and lung HYP content ($R^2 = 0.9631$, $P < 0.0001$) (Fig. 6c).

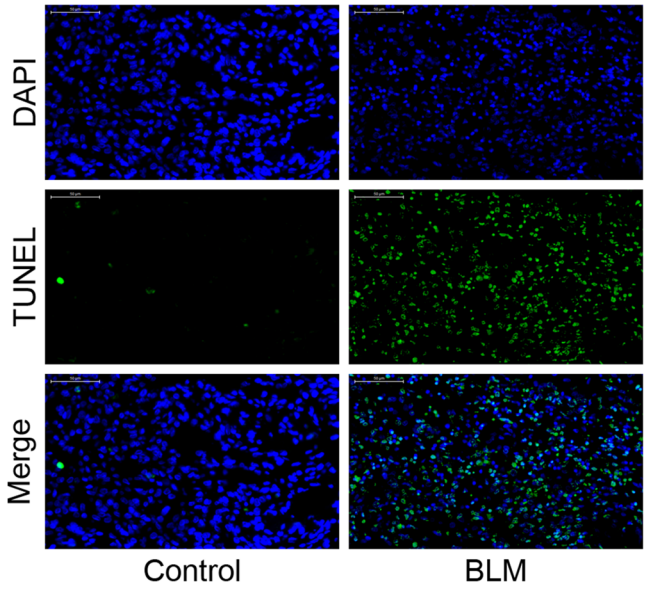

Fig. 2. Immunofluorescence staining analysis of lung tissues harvested from rats 21 days after administration of saline or BLM. Scale bars = 50 μm. *BLM* bleomycin.

Conversely, such a correlation was not found between [^{18}F]FDG uptake and lung HYP content after administration of BLM (Fig. 6d).

Discussion

In this study, we investigated the capabilities of PET/CT imaging of [^{18}F]ML-10 to noninvasively quantify and characterize the progression of BLM-induced pulmonary fibrosis in a rat model.

Bleomycin induction was the most commonly used strategy to generate pulmonary fibrosis in a rat model. In the previous researches, after intratracheal instillation of BLM, neutrophilic and lymphocytic alveolitis occurred in lung tissues within the first week and then inflammatory cells were cleared, proliferation of fibroblasts and excessive accumulation of extracellular matrix occurred at the later phase of this disease model. Obvious pulmonary fibrosis was detected histologically and biochemically at day 14, with maximal fibrotic activity noted around days 21–28 [6, 29, 30]. In our experiment, Masson trichrome staining helped to confirm the pathologic process of lung fibrosis. Compared with the control group, lung tissues of the BLM group showed significant histologic modifications, including over-proliferation of fibroblasts and excessive deposition of collagens and extracellular matrix proteins. Moreover, the fibrotic areas of lung tissues increased with increasing BLM administration time. According to histologic staining, fibrosis score of the BLM group was significantly higher than that of the control group at day 21 after instillation. In addition, we assessed the dynamic changes of collagen content in the lung tissues of the two groups by measuring lung HYP content. Comparison of lung HYP content between the two groups also demonstrated increasing pulmonary fibrosis in the lung tissues of BLM-treated rats from day 7 to day 28 after instillation. All these data confirmed that the BLM-induced rat pulmonary fibrosis model was successfully established and a strong fibrotic response occurred at the later period of this disease model.

The pathogenesis of pulmonary fibrosis is still unclear [1]. Previous study demonstrated that apoptosis of type II pneumocytes occurred in normal alveoli of IPF patients and could be crucial for the pathogenesis of IPF [22]. In this experiment, we investigated the presence of apoptotic cells and assessed the apoptosis rate of lung tissues by TUNEL staining and flow cytometry. TUNEL staining of lung tissues in both groups demonstrated that apoptotic cells accumulated in lung sections of the BLM group. Furthermore, flow cytometry results indicated that apoptosis rate of the BLM group increased with increasing BLM administration time. These results demonstrated that apoptotic cells were present in fibrotic

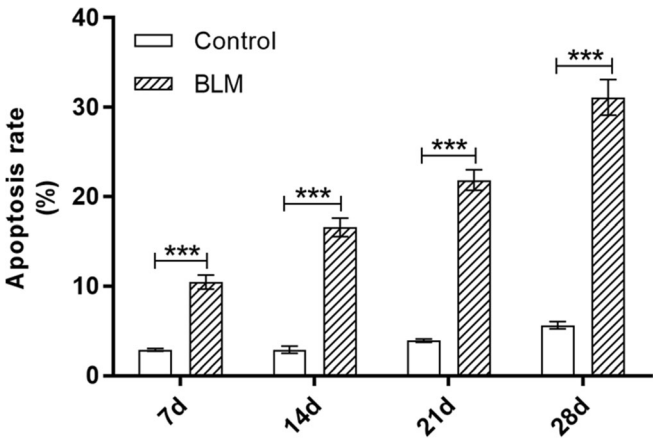

Fig. 3. Apoptosis rate of lung tissues in the control and BLM groups at 7, 14, 21, and 28 days after instillation ($n = 3$ per group for days 7, 14, 21, and 28, respectively). All data are given as means ± standard deviations. $^{*}P < 0.05$, $^{**}P < 0.01$, $^{***}P < 0.001$. *BLM* bleomycin.

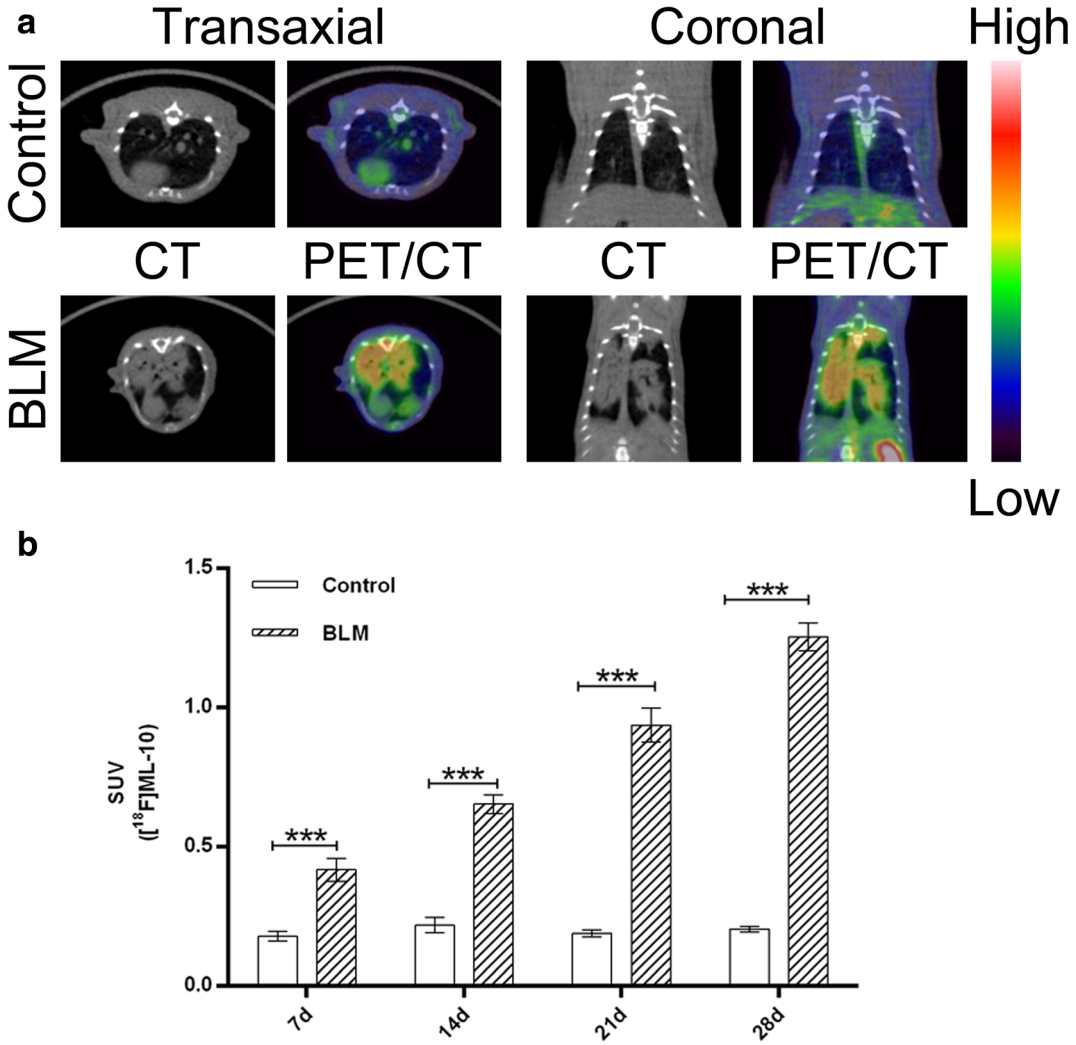

Fig. 4. Increased [^{18}F]ML-10 uptake in BLM-treated rats. PET/CT was performed 60 min after injection of [^{18}F]ML-10 (37 MBq/kg) *via* tail vein. **a** Representative [^{18}F]ML-10 PET/CT images in the control and BLM groups at day 28 after instillation (the red arrows indicate fibrotic lung tissues). **b** Mean uptake of [^{18}F]ML-10 within lungs at 7, 14, 21, and 28 days after administration of saline or BLM. All data are given as means ± standard deviations. $^{*}P < 0.05$, $^{**}P < 0.01$, $^{***}P < 0.001$. *BLM* bleomycin.

lung tissues of this disease model. Altogether, these data mentioned above helped confirm the induction of a strong fibrotic activity and significantly enhanced lung cell apoptosis during the progression of this disease in a rat model. Therefore, molecular imaging of apoptosis may have important implications for noninvasive diagnosis of pulmonary fibrosis and evaluation of fibrotic activity.

Apoptosis is a mode of programmed cell death and it is characterized by nuclear breakup and cell shrinkage [31]. A characteristic feature of the Aposense family is that they can pass across the plasma membrane and selectively accumulate in the apoptotic cells [32]. As a member of Aposense family, [^{18}F]ML-10 had been confirmed to selectively accumulate in apoptotic cells and was used for *in vivo* imaging of apoptosis in animal models of apoptosis [23, 32]. In this study, [^{18}F]ML-10 PET data demonstrated that the areas of maximal [^{18}F]ML-10 uptake in the BLM group corresponded to CT changes, with predominant honeycombing and reticulation, which were associated with fibrotic changes of lung tissues. Comparison of [^{18}F]ML-10 uptake between the two groups demonstrated that [^{18}F]ML-10 uptake of lung tissues increased at the early inflammatory phase and persisted at the later fibrotic phase of this disease model. Moreover, [^{18}F]ML-10 uptake in lung tissues increased in proportion to fibrosis progression from day 7 to day 28 after instillation. Thus, we hypothesized that apoptotic PET imaging with [^{18}F]ML-10 could be used for assessing the fibrotic activity during the progression of rat pulmonary fibrosis. Our results showed that [^{18}F]ML-10 uptake of lung tissues showed a strong positive correlation with apoptosis rate as well as with lung HYP content, a major component of collagen and a marker of fibrosis [6, 24, 28]. We then concluded that lung uptake of [^{18}F]ML-10 increased in proportion to the apoptosis rate and fibrotic

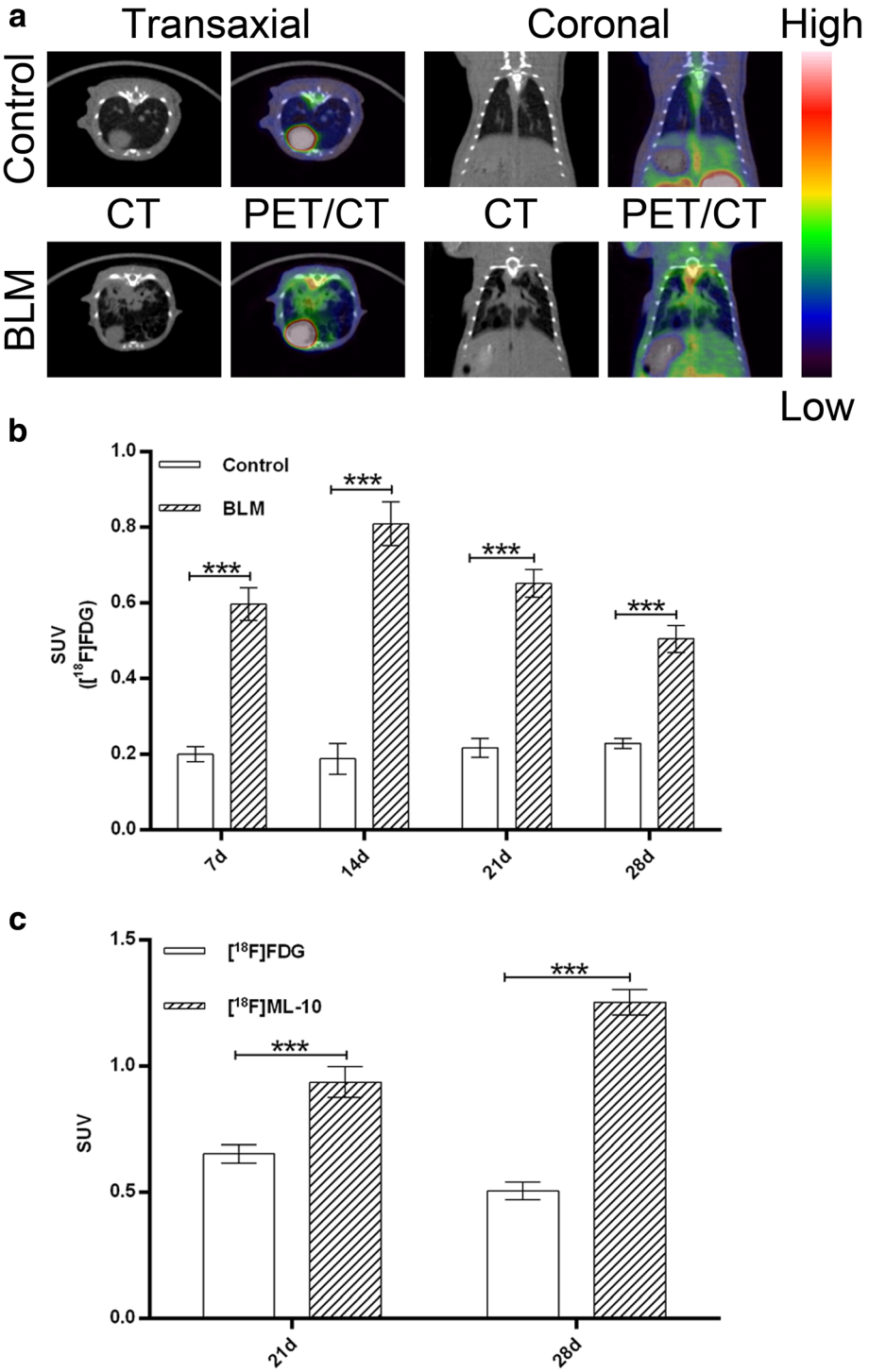

Fig. 5. Early increased [^{18}F]FDG uptake in BLM-treated rats. PET/CT was performed 60 min after injection of [^{18}F]FDG (37 MBq/kg) *via* tail vein. **a** Representative [^{18}F]FDG PET/CT images in the control and BLM groups at day 14 after instillation (the red arrows indicate fibrotic lung tissues). **b** Mean uptake of [^{18}F]FDG within lungs at 7, 14, 21, and 28 days after administration of saline or BLM ($n = 3$ per group for days 7, 14, 21, and 28, respectively). **c** Bar chart shows difference in the lung uptake between [^{18}F]ML-10 PET and [^{18}F]FDG PET at days 21 and 28 after BLM instillation. All data are given as means ± standard deviations. $^{*}P < 0.05$, $^{**}P < 0.01$, $^{***}P < 0.001$. *BLM* bleomycin.

activity during the progression of rat pulmonary fibrosis. Altogether, these results highlighted that PET imaging of [^{18}F]ML-10 could be used for noninvasive diagnosis of rat pulmonary fibrosis and assessment of fibrotic activity.

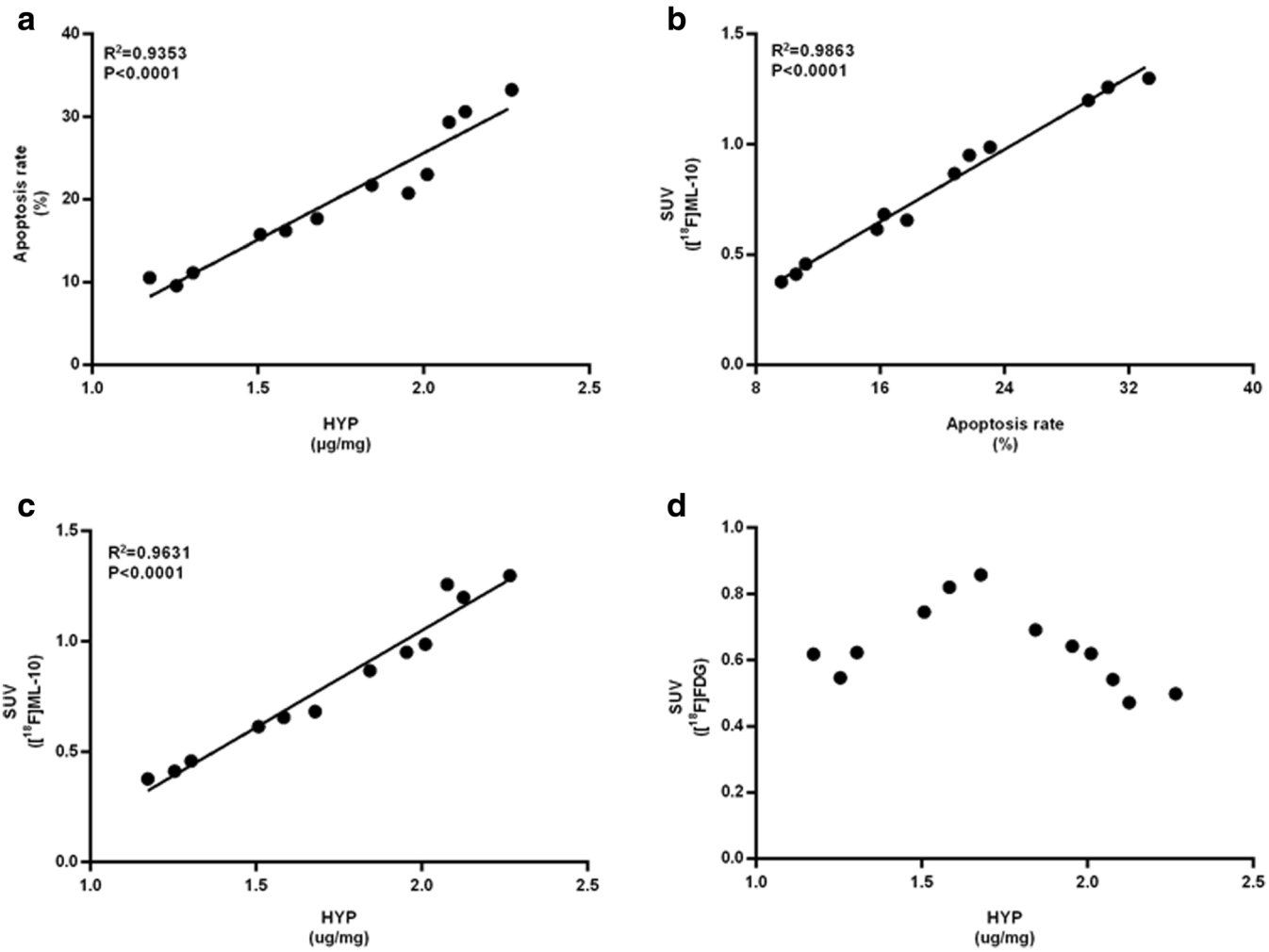

Fig. 6. Positive correlation between pulmonary fibrosis and cell apoptosis and [^{18}F]ML-10 uptake, but not with [^{18}F]FDG uptake (HYP, apoptosis rate, [^{18}F]ML-10 uptake, and [^{18}F]FDG uptake assessed at 7, 14, 21, and 28 days after administration of BLM). **a** Graph shows correlation between marker of fibrosis (HYP) and apoptosis rate. **b** Graph shows correlation between apoptosis rate and [^{18}F]ML-10 uptake. **c** Graph shows correlation between marker of fibrosis (HYP) and [^{18}F]ML-10 uptake. **d** No correlation between marker of fibrosis (HYP) and [^{18}F]FDG uptake. *BLM* bleomycin.

Recent studies reported that [^{18}F]FDG could be used for molecular imaging of pulmonary fibrosis in IPF patients and animal models [6, 8, 11, 13, 14, 19]. Our data confirmed that [^{18}F]FDG uptake of lung tissues increased significantly at the early inflammatory phase and slowly decreased at the late fibrotic phase of rat pulmonary fibrosis, which was well in alignment with findings in previous animal [^{18}F]FDG PET/CT studies [6, 19]. Furthermore, no correlation was observed between [^{18}F]FDG uptake of lung tissues and fibrotic activity. Compared with [^{18}F]FDG PET/CT, our study found that PET/CT with [^{18}F]ML-10 could better reflect the fibrotic process of this disease and assess the severity and activity of pulmonary fibrosis.

Our experiment had certain limitations. This study was performed in BLM-induced pulmonary fibrosis rat model, which might not reflect all types of lung fibrosis. Therefore, further studies of PET/CT imaging with [^{18}F]ML-10 in other types of pulmonary fibrosis models and clinical trials would be required to further demonstrate the capabilities of [^{18}F]ML-10 for pulmonary fibrosis imaging.

Conclusions

Overall, our study demonstrated that PET with small-molecule apoptotic radiotracer, [^{18}F]ML-10, could be a potential tool to noninvasively diagnose BLM-induced pulmonary fibrosis, characterize the progression of pulmonary fibrosis, and assess the disease activity in a rat model.

Once further validated in animal and clinical studies, [^{18}F]ML-10 PET/CT could be a promising method for diagnosis of pulmonary fibrosis, evaluation of fibrotic activity and assessment of efficacy of antifibrotic treatments.

Author Contributions. Xianhong Xiang and Ganghua Tang had full access to all of the data in the study and take responsibility for the integrity of the data and the accuracy of the data analysis. Ying Xiong and Dahong Nie contributed to designing this study, collecting samples, carrying out experiments, and writing the manuscript. Shaoyu Liu, Hui Ma, and Shu Su contributed to collecting samples and revising the manuscript. Aixia Sun, Jing Zhao, and Zhanwen Zhang contributed to revising the manuscript. All authors have approved the final article.

Funding. This work was supported by the National Natural Science Foundation of China (No. 81571704, No. 81371584, No. 81671719), the Science and Technology Foundation of Guangdong Province (No. 2014A020210008, No. 2013B021800264, No. 2016B090920087), the Science and Technology Planning Project Foundation of Guangzhou (No. 201604020169, No. 201510010145), and the Natural Science Foundation of Guangdong Province (No. 2015A030313067).

Compliance with Ethical Standards

Conflict of Interest

The authors declare that they have no conflict of interest.

References

1. King TE Jr, Pardo A, Selman M (2011) Idiopathic pulmonary fibrosis. Lancet 378:1949–1961
2. Nalysnyk L, Cid-Ruzafa J, Rotella P, Esser D (2012) Incidence and prevalence of idiopathic pulmonary fibrosis: review of the literature. Eur Respir Rev 21:355–361
3. du Bois RM (2010) Strategies for treating idiopathic pulmonary fibrosis. Nat Rev Drug Discov 9:129–140
4. Raghu G, Collard HR, Egan JJ, Martinez FJ, Behr J, Brown KK, Colby TV, Cordier JF, Flaherty KR, Lasky JA, Lynch DA, Ryu JH, Swigris JJ, Wells AU, Ancochea J, Bouros D, Carvalho C, Costabel U, Ebina M, Hansell DM, Johkoh T, Kim DS, King te Jr, Kondoh Y, Myers J, Müller NL, Nicholson AG, Richeldi L, Selman M, Dudden RF, Griss BS, Protzko SL, Schünemann HJ, ATS/ERS/JRS/ALAT Committee on Idiopathic Pulmonary Fibrosis (2011) An official ATS/ERS/JRS/ALAT statement: idiopathic pulmonary fibrosis: evidence-based guidelines for diagnosis and management. Am J Respir Crit Care Med 183:788–824
5. Raghu G, Anstrom KJ, King TE Jr et al (2012) Prednisone, azathioprine, and N-acetylcysteine for pulmonary fibrosis. N Engl J Med 366:1968–1977
6. Bondue B, Sherer F, Van Simaeys G et al (2015) PET/CT with [^{18}F]FDG- and [^{18}F]FBEM-labeled leukocytes for metabolic activity and leukocyte recruitment monitoring in a mouse model of pulmonary fibrosis. J Nucl Med 56:127–132
7. Blodgett TM, Meltzer CC, Townsend DW (2007) PET/CT: form and function. Radiology 242:360–385
8. Win T, Lambrou T, Hutton BF, Kayani I, Screaton NJ, Porter JC, Maher TM, Endozo R, Shortman RI, Lukey P, Groves AM (2012) [^{18}F]Fluorodeoxyglucose positron emission tomography pulmonary imaging in idiopathic pulmonary fibrosis is reproducible: implications for future clinical trials. Eur J Nucl Med Mol Imaging 39:521–528
9. Ambrosini V, Zompatori M, De Luca F et al (2010) ^{68}Ga-DOTANOC PET/CT allows somatostatin receptor imaging in idiopathic pulmonary fibrosis: preliminary results. J Nucl Med 51:1950–1955
10. Wallace WE, Gupta NC, Hubbs AF et al (2002) Cis-4-[^{18}F]fluoro-L-proline PET imaging of pulmonary fibrosis in a rabbit model. J Nucl Med 43:413–420
11. Umeda Y, Demura Y, Ishizaki T, Ameshima S, Miyamori I, Saito Y, Tsuchida T, Fujibayashi Y, Okazawa H (2009) Dual-time-point [^{18}F]FDG PET imaging for diagnosis of disease type and disease activity in patients with idiopathic interstitial pneumonia. Eur J Nucl Med Mol Imaging 36:1121–1130
12. El-Chemaly S, Malide D, Yao J et al (2013) Glucose transporter-1 distribution in fibrotic lung disease: association with [^{18}F]-2-fluoro-2-deoxyglucose-PET scan uptake, inflammation, and neovascularization. Chest 143:1685–1691
13. Groves AM, Win T, Screaton NJ, Berovic M, Endozo R, Booth H, Kayani I, Menezes LJ, Dickson JC, Ell PJ (2009) Idiopathic pulmonary fibrosis and diffuse parenchymal lung disease: implications from initial experience with [^{18}F]FDG PET/CT. J Nucl Med 50:538–545
14. Meissner HH, Soo Hoo GW, Khonsary SA, Mandelkern M, Brown CV, Santiago SM (2006) Idiopathic pulmonary fibrosis: evaluation with positron emission tomography. Respiration 73:197–202
15. Lavalaye J, Grutters JC, van de Garde EM et al (2009) Imaging of fibrogenesis in patients with idiopathic pulmonary fibrosis with cis-4-[^{18}F]-Fluoro-L: -proline PET. Mol Imaging Biol 11:123–127
16. Jones HA, Valind SO, Clark IC, Bolden GE, Krausz T, Schofield JB, Boobis AR, Haslett C (2002) Kinetics of lung macrophages monitored in vivo following particulate challenge in rabbits. Toxicol Appl Pharmacol 183:46–54
17. Bellani G, Caironi P (2011) Lung imaging during acute respiratory distress syndrome: CT- and PET-scanning. Trends in Anaesthesia and Critical Care 1:203–209
18. Win T, Screaton NJ, Porter J, Endozo R, Wild D, Kayani I, Dickson J, Shortman RI, Reubi JC, Ell PJ, Groves AM (2012) Novel positron emission tomography/computed tomography of diffuse parenchymal lung disease combining a labeled somatostatin receptor analogue and 2-deoxy-2[^{18}F]fluoro-D-glucose. Mol Imaging 11:91–98
19. Jones HA, Schofield JB, Krausz T et al (1998) Pulmonary fibrosis correlates with duration of tissue neutrophil activation. Am J Respir Crit Care Med 158:620–628
20. Taylor RC, Cullen SP, Martin SJ (2008) Apoptosis: controlled demolition at the cellular level. Nat Rev Mol Cell Biol 9:231–241
21. Fine A, Janssen-Heininger Y, Soultanakis RP, Swisher SG, Uhal BD (2000) Apoptosis in lung pathophysiology. Am J Phys Lung Cell Mol Phys 279:L423–L427
22. Barbas-Filho JV, Ferreira MA, Sesso A, Kairalla RA, Carvalho CR, Capelozzi VL (2001) Evidence of type II pneumocyte apoptosis in the pathogenesis of idiopathic pulmonary fibrosis (IFP)/usual interstitial pneumonia (UIP). J Clin Pathol 54:132–138
23. Reshef A, Shirvan A, Akselrod-Ballin A, Wall A, Ziv I (2010) Small-molecule biomarkers for clinical PET imaging of apoptosis. J Nucl Med 51:837–840
24. Zhang K, Si XP, Huang J, Han J, Liang X, Xu XB, Wang YT, Li GY, Wang HY, Wang JH (2016) Preventive effects of Rhodiola rosea L. on bleomycin-induced pulmonary fibrosis in rats. Int J Mol Sci 17:879
25. Tang H, Gao L, Mao J, He H, Liu J, Cai X, Lin H, Wu T (2016) Salidroside protects against bleomycin-induced pulmonary fibrosis: activation of Nrf2-antioxidant signaling, and inhibition of NF-kappaB and TGF-beta1/Smad-2/-3 pathways. Cell Stress Chaperones 21:239–249
26. Liu S, Nie D, Jiang S, Tang G (2017) Efficient automated synthesis of 2-(5-[^{18}F]fluoropentyl)-2-methylmalonic acid ([^{18}F]ML-10) on a commercial available [^{18}F]FDG synthesis module. Appl Radiat Isot 123:49–53
27. Ashcroft T, Simpson JM, Timbrell V (1988) Simple method of estimating severity of pulmonary fibrosis on a numerical scale. J Clin Pathol 41:467–470
28. Sener G, Topaloglu N, Sehirli AO et al (2007) Resveratrol alleviates bleomycin-induced lung injury in rats. Pulm Pharmacol Ther 20:642–649
29. Janick-Buckner D, Ranges GE, Hacker MP (1989) Alteration of bronchoalveolar lavage cell populations following bleomycin treatment in mice. Toxicol Appl Pharmacol 100:465–473
30. Moore BB, Hogaboam CM ((2008)) Murine models of pulmonary fibrosis. Am J Physiol Lung Cell Mol Physiol 294:L152–L160
31. Kadirvel M, Fairclough M, Cawthorne C, Rowling EJ, Babur M, McMahon A, Birkket P, Smigova A, Freeman S, Williams KJ, Brown G (2014) Detection of apoptosis by PET/CT with the diethyl ester of [^{18}F]ML-10 and fluorescence imaging with a dansyl analogue. Bioorg Med Chem 22:341–349
32. Chopra A (2004) 2-(5-[18F]Fluoro-pentyl)-2-methyl-malonic acid (ML-10), molecular imaging and contrast agent database (MICAD). National Center for Biotechnology Information (US), Bethesda